반도체디스플레이기술학회지 제22권 제3호(2023년 9월)
Journal of the Semiconductor & Display Technology, Vol. 22, No. 3. September 2023.

Development of a Plate-type Megasonic with Cooling Pins for Sliced Ingot Cleaning

Hyunse Kim[*,**†] **and Euisu Lim**[*]

[*†] Innovative Energy Machinery Research Division, Korea Institute of Machinery and Materials,
[**]Department of Mechanical Engineering, University of Science and Technology

ABSTRACT

In this article, a plate-type megasonic cleaning system with cooling pins is proposed for the sliced ingot, which is a raw material of silicon (Si) wafers. The megasonic system is operated with a lead zirconate titanate (PZT) actuator, which has high electric resistance, thus when it is being operated, it dissipates much heat. So this article proposes a megasonic system with cooling pins. In the design process, finite element analysis was performed and the results were used for the design of the waveguide. The frequency with the maximum impedance value was 998 kHz, which agreed well with the measured value of 997 kHz with 0.1 % error. Based on the results, the 1 MHz waveguide was fabricated. Acoustic pressures were measured, and analyzed. Finally, cleaning tests were performed, and 90 % particle removal efficiency (PRE) was achieved over 10 W power. These results imply that the developed 1 MHz megasonic will effectively clean sliced ingot wafer surfaces.

Key Words : Megasonic, Finite element method (FEM), Sliced Ingot, Cleaning, Impedance

1. Introduction

In industrial areas, ultrasonics are widely applied to fabrication, cleaning, food, chemical reaction, etc.[1]. In the manufacturing process, it is utilized in ultrasonic vibration-assisted drilling[2,3]. It can also assist in the turning process of high-hardness metals[4]. Jung et al. researched into the effect of ultrasonic vibration on drawing force[5]. Regarding cleaning, Park et al. reported the comparison of cleaning effects of gas and vapor bubbles in ultrasonic fields[6]. Among them, megasonics are proposed to use in a semiconductor cleaning process[7]. Another application is ultrasonic peening milling [8]. When milling metals, mechanical vibration can be applied to aid the milling processes. It can be also used as a flow sensor in semiconductor process[9]. Ha et al. applied the ultrasonic power for the Mist-Chemical Vapor Deposition (CVD) process[10,11].

Recent research has applied megasonic frequency, which is frequency above 1 MHz that is higher than the general ultrasonic frequency near 20 kHz, to the semiconductor cleaning process[12,13]. Compared to ultrasonics, high-frequency has the strong advantage of lower displacement, which can be used in sensitive structures, such as micro or nano-patterns. We previously developed an L-type waveguide megasonic system for the cleaning of nano-scale patterns[14]. Chu et al. compared the ultrasonic and megasonic cleaning of nanoscale patterns in ammonia hydroxide solutions[15]. Ochiai et al. researched about a numerical analysis of a single bubble behavior in a megasonic field by a simulation[16]. In addition, Han et al. performed an analysis of a sonoluminescence signal from megasonic irradiated gas-containing aqueous solutions[17]. And Li et al. analyzed a mechanism of a megasonic and a brush cleaning processes for silicon substrates after a chemical mechanical polishing process[18]. Lastly, Zhang et al. reported non-contact post-CMP megasonic cleaning results of cobalt wafers[19]. But these researches are lacking in the development of the megasonic system.

The megasonic system is generally operated with a lead

†E-mail: hkim@kimm.re.kr

zirconate titanate (PZT) actuator. The PZT actuator has high electric resistance, so when it is being operated, it dissipates much heat. So in this work, we propose a megasonic system with aluminum (Al) cooling pins. The Al pins are configured with the first step of the Al waveguide.

The plate-type megasonic cleaning system is proposed for the sliced ingot, which is a raw material of silicon (Si) wafers. The megasonic system is operated with a lead zirconate titanate (PZT) actuator, which is composed of an aluminum (Al) and a quartz waveguide. In the design step, finite element analysis was performed and the results were used for the design of the waveguide. The frequency with the maximum impedance value was 1,000 kHz, which agreed well with the measured value of 997 kHz with 0.3 % error. At this time, acoustic pressures were measured, and the PRE was also measured through cleaning wafer tests. Based on the results, the 1 MHz waveguide was fabricated. These results imply that the developed 1 MHz megasonic will be helpful for the effective cleaning of sliced ingot wafer surfaces.

2. Design of the Megasonic Waveguide

2.1 Plate-type megasonic design

Fig. 1(a) illustrates the structure of the plate-type megasonic, while Fig. 1(b) shows the fabricated plate-type megasonic. The operating power is supplied by an electric generator, which is shown in Fig. 2. The megasonic part is composed of a PZT actuator, an aluminum plate for cooling and a quartz waveguide. For the basic design of the system, the following equation was used:

$$v = f \cdot \lambda \tag{1}$$

where, v is the velocity of the wave, f the frequency, and λ the wavelength. The first step of the waveguide is the aluminum (Al) cylinder. Thus, using the velocity of Al (v_1=5,050 m/s), the λ_1 for the operating frequency of 1 MHz could be obtained as 5.05 mm. The maximum displacement can be obtained at each multiple of half λ. So we multiplied 14 by the half λ_1, and the calculated length was 35.35 mm.

Using the same procedures, the λ_2 of the quartz could be obtained as 5.98 mm, where the velocity of quartz was 5,980 m/s. The maximum displacement can be obtained at each multiple of half λ. Thus, the half λ_2 is 2.99 mm, and we used this value as the waveguide length.

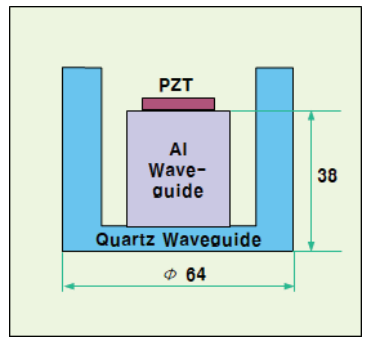

(a)

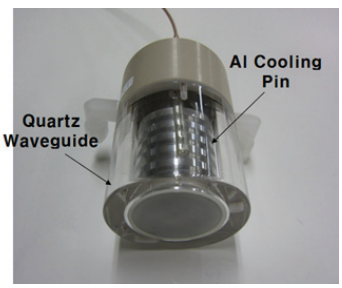

(b)

Fig. 1. (a) Structure of the plate-type quartz megasonic and (b) fabricated megasonic.

Fig. 2. Electric generator.

2.2 Finite element analysis

For the analysis of the PZT actuator, FEM was performed using commercial Ansys software. The actuator was modelled axis-symmetrically, and the harmonic analysis was processed. We tried to find more accurate dimensions through the FEM by slightly changing each dimension. Fig. 3(a) shows the FEM PZT model, while Fig. 3(b) shows the PZT impedance graph obtained. It was modelled axis-symmetrically, and the voltages are given at the top and bottom sides. The maximum impedance value was found at 1 MHz, which value was set as a design value. After fabricating the PZT, the impedance was

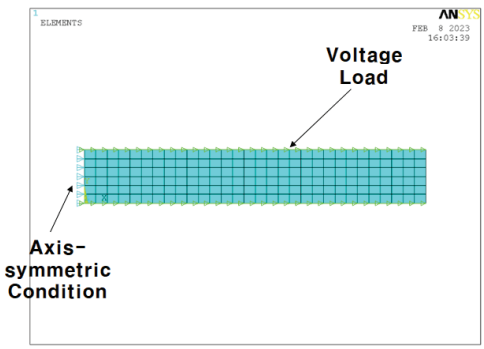

(a)

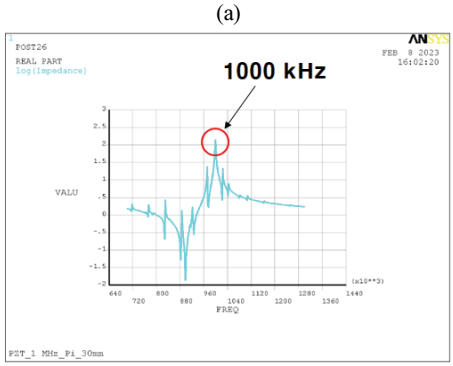

(b)

Fig. 3. (a) PZT model and (b) FEM impedance graph.

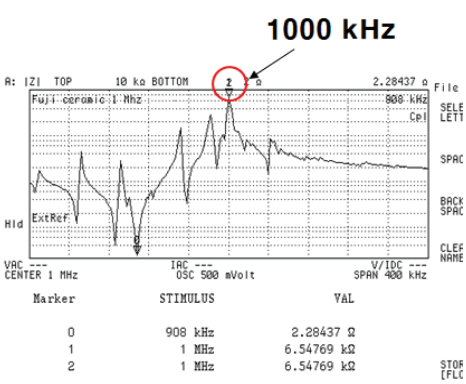

Fig. 4. The measured PZT impedance graph.

measured, and it coincided with the analysis result of 1 MHz, as shown in Fig. 4 (Impedance Analyzer, Agilent Inc.).

Secondly, the PZT with a cooling pin was designed. Due to the high heat from the PZT, we adapted aluminum (Al) cooling pins for the Al waveguide, instead of a quartz material, so that the Al cooling part could transfer the megasonic energy, and cool down the heat from the actuator. Next, the second quartz waveguide was attached at the end of the cooling part.

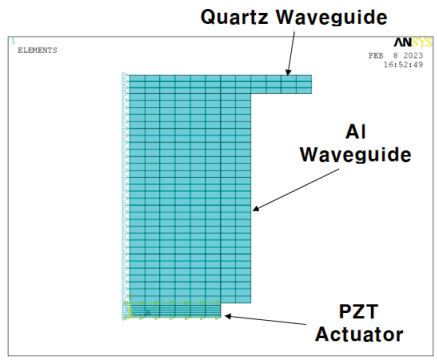

(a)

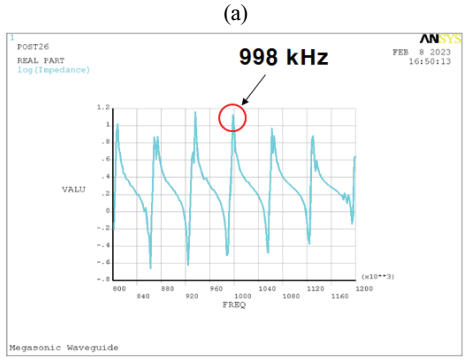

(b)

Fig. 5. (a) Analysis model of the Al and quartz waveguide and (b) the impedance graph.

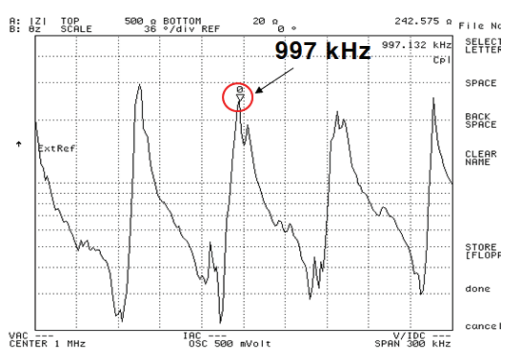

Fig. 6. Measured impedance graph of the 1 MHz.

The calculated dimensions of the previous chapter were utilized. For the analysis of the cooling part and the quartz waveguide, it was modelled axis-symmetrically, and the voltage load was applied to the actuator. Fig. 5(a) shows the analysis model of the quartz waveguide, and Fig. 5(b) the impedance graph, which result showed 998 kHz peak frequency. Using these results, the megasonic was fabricated, and the impedance was measured. Fig. 6 shows the result, and

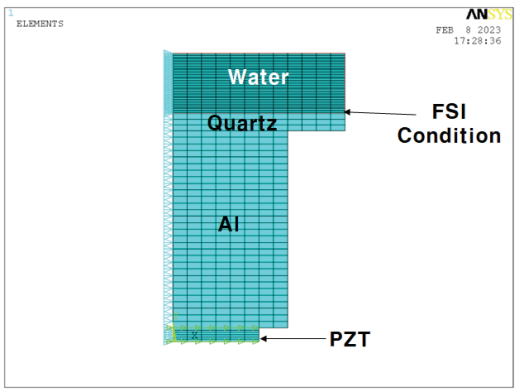

(a)

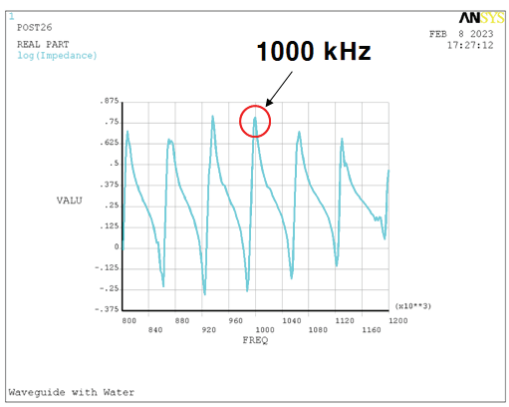

(b)

Fig. 7. (a) Analysis model of the quartz waveguide with water and (b) impedance graph.

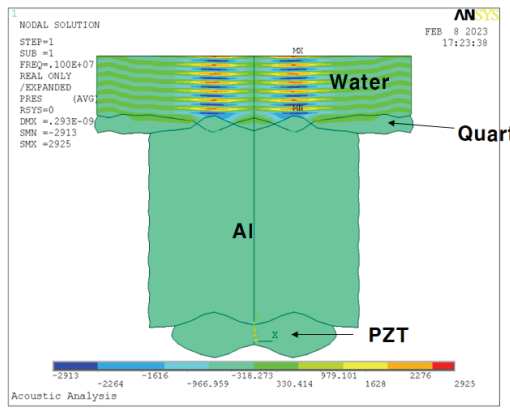

(a)

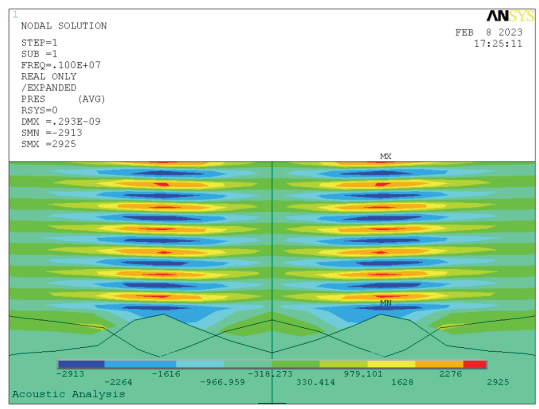

(b)

Fig. 8. Acoustic pressure distributions of (a) the waveguide with water and (b) magnified view.

the peak value was 997 kHz, which agreed well with the analysis result with 0.1 % error.

For the last analysis, the water was modelled at the end of the waveguide, as shown in Fig. 7(a). As a result, the peak frequency was obtained as 1 MHz, which is shown in Fig. 7(b). Fig. 8(a) shows the acoustic pressure distributions of the waveguide with water, while Fig. 8(b) provides a magnified view. The red area indicates higher acoustic pressure, while the blue area indicates lower pressure. From these results, we can expect well- distributed pressures at the end of the waveguide.

3. Experiment

The megasonic performance can be evaluated by measuring the acoustic pressure and a particle removal test. Fig. 9 shows the experimental setup (Acoustic Pressure Measurement System, AcouLab Inc.). Acoustic pressure can be measured in water with a hydrophone sensor. In air, microphones are generally used to measure acoustic pressure, while in water, hydrophones are used. The intensity of the acoustic pressure can be used to represent the system performance.

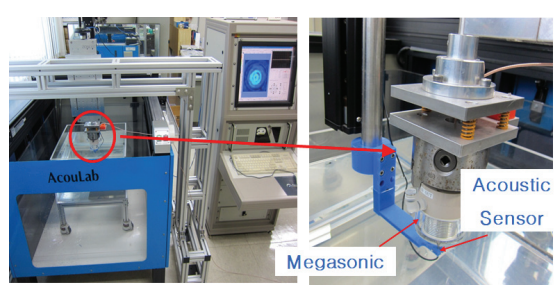

Fig. 9. Experimental setup for acoustic pressure measurement.

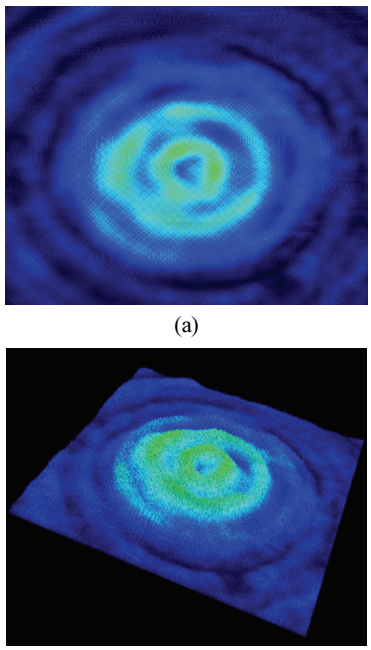

(a) (b)

Fig. 10. Acoustic pressure distributions of the waveguide: (a) 2D view and (b) 3D view.

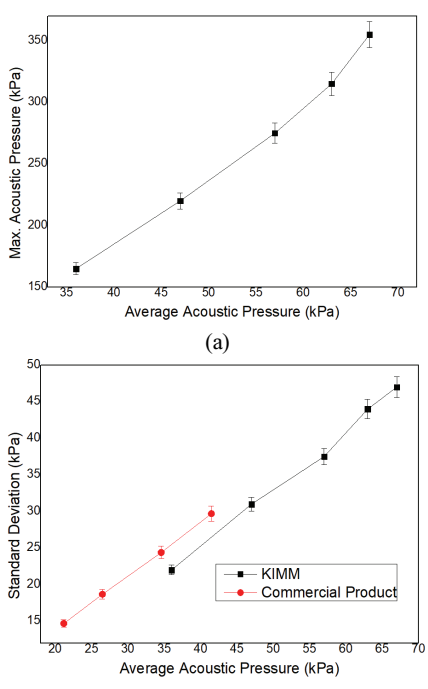

(a) (b)

Fig. 11. Acoustic pressures measurement results of (a) the maximum and (b) standard deviation.

Fig. 12. Cleaning test equipment.

The developed megasonic is immersed in a water tank for the experiment. While supplying electricity to the PZT on the waveguide, the bottom surface emits acoustic power to the water. Then to measure the entire bottom surface, the hydrophone sensor moves in a zig-zag with a 0.05 mm step. The measured values were transferred to the personal computer (PC) for saving and analysis. We repeated the tests with different input powers. Fig. 10(a) shows the measured plot with two-dimensional (2D) view, while Fig. 10(b) shows the three-dimensional (3D) view. The blue bright area represents high acoustic pressure, while the black and dark areas represent low pressure.

The measured data were analysed, and the average, maximum, and standard deviation were calculated. Fig. 11(a) shows the maximum vs. average, while Fig. 11(b) shows the standard deviation vs. average. As the input power increases, the average output pressure rises. In addition, when the average has incremental values, the maximum acoustic pressure also increases. Finally, the index of good distribution is the standard deviation, and it also shows a tendency of rising with the added averages. Compared to a commercial product (type-A), we could obtain 10 % better standard deviation values.

Secondly, the developed megasonic was designed for cleaning sub-micron particles, so the cleaning test was per-

formed by counting deposited nano-particles on a Si wafer (8 inch Si Wafer, thickness = 525 μm), and the remained numbers after cleaning. Cleaning test using silica particles was performed. Fig. 12 shows the cleaning equipment, which is composed of the cleaning system, and the surface analyzer. The cleaning test performed the following procedures: (1) particle deposition, (2) particle counting, (3) cleaning, and (4) remained particle counting. The particles were counted by our surface analyzer system, which uses laser for counting. In the cleaning system, the particle cleaning process is performed using our developed megasonic. After cleaning, the remaining particles were counted. Fig. 13(a) shows the scanned particle images before cleaning, and Fig. 13(b) the images after. Over 90 % of particle removal efficiency (PRE) was achieved over 10 W power, as shown in Fig. 14.

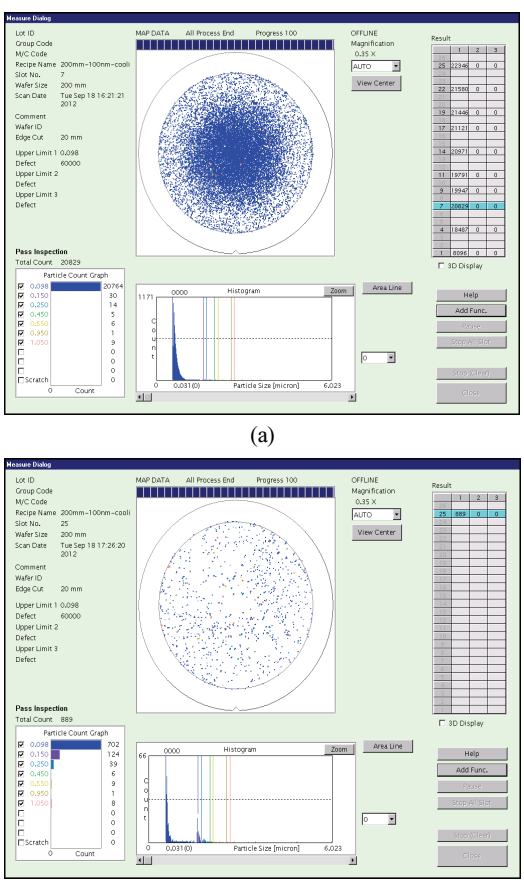

Fig. 13. Cleaning test results of (a) before and (b) after.

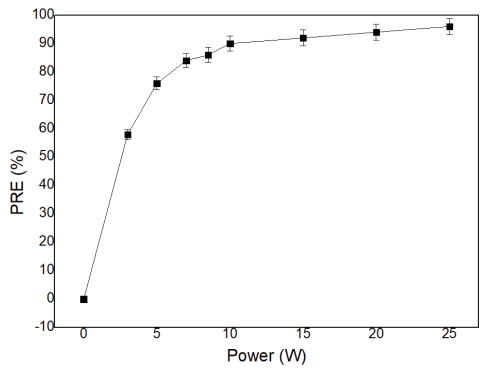

Fig. 14. PRE graph.

4. Conclusion

In this paper, the plate-type megasonic cleaning system with Al cooing pins was proposed for the sliced ingot, which is a raw material of Si wafers. The megasonic system is operated with the PZT actuator. It is composed of the Al and the quartz waveguide. In the design process, finite element analysis was performed, and the results were used for the design of the waveguide. The frequency with the maximum impedance value was 998 kHz, which agreed well with the measured value of 997 kHz with 0.1 % error. Based on the results, the 1 MHz waveguide was fabricated. Acoustic pressures were measured, and analyzed. Finally, cleaning tests were performed, and 90 % particle removal efficiency (PRE) was achieved over 10 W power. These results imply that the developed 1 MHz megasonic will be helpful for the cleaning of sliced ingot wafer surfaces effectively.

Acknowledgement

We are grateful to the contribution of Dr. Yang Lae Lee at Korea Institute of Machinery and Materials. This research was funded by the Korea Institute of Energy Technology Evaluation and Planning (KETEP), under the Korea government Ministry of Trade, Industry and Energy (Project, NE4560). And it was also supported by a research project (NK243C) of the Korea Institute of Machinery and Materials (KIMM).

References

1. Gallego-Juarez, J. A., and Graff, K. F., “Power Ultrasonics: Applications of High-intensity Ultrasound,”

Woodhead Publishing, Cambridge, UK, 2014.
2. Liu, Y., Geng, D., Shao, Z., Zhou, Z., Jiang, X., and Zhang, D., "A Study on Strengthening and Machining Integrated Ultrasonic Peening Drilling of Ti-6Al-4V," Materials & Design, Vol. 212, p. 110238, 2021.
3. Liu, Y., Ma, L., Liu, F., Fu, B., and Yao, J., "A Novel Model of Vibration Plowing Effect for Longitudinal Ultrasonic Vibration-assisted Drilling," Journal of Manufacturing Processes, Vol. 87, No. 3, pp. 65-80, 2023.
4. Airao, J., Nirala, C. K., Bertolini, R., Krolczyk, G. M., and Khanna, N., "Sustainable Cooling Strategies to Reduce Tool Wear, Power Consumption and Surface Roughness during Ultrasonic Assisted Turning of Ti-6Al-4V," Tribology International, Vol. 169, p. 107494, 2022.
5. Jung, H. K., Park, J. K., Kim, H. C., and Kim, J.-B., "An Investigation into the Effect of Ultrasonic Vibration on Drawing Force," Journal of the Korean Society for Precision Engineering, Vol. 35, No. 5, pp. 493-498, 2018.
6. Park, R., Choi, M., Park, E. H., Shon, W.-J., Kim, H.-Y., Kim, W., "Comparing Cleaning Effects of Gas and Vapor Bubbles in Ultrasonic Fields," Ultrason. Sonochem. Vol. 76, p. 105618, 2021.
7. Kanegsberg, B. and Kanegsberg, E., "Handbook for Critical Cleaning," CRC Press, Boca Raton, 2000.
8. Yin, X., Li, X., Liu, Y., Geng, D., and Zhang, D., "Surface Integrity and Fatigue Life of Inconel 718 by Ultrasonic Peening Milling," Journal of Materials Research and Technology, Vol. 22, pp. 1392-1409, 2023.
9. Bae, I. J. and Lee, E. S., "Improvement of Measuring Stability of Amplitude Attenuation by the Bubble in Ultrasonic Flow-meter for Semiconductor Process," Journal of the Korean Society for Precision Engineering, Vol. 36, No. 9, pp. 843-849, 2019.
10. Ha, J., Park S., Lee, H., Shin, S., and Byun, C., "Uniformity Prediction of Mist-CVD Ga_2O_3 Thin Film using Particle Tracking Methodology," J. Semiconductor & Display Technology, Vol. 21, No. 3., pp. 101-104, 2022.
11. Ha, J., Lee, H., Park S., Shin, S., and Byun, C., "Computational Fluid Dynamics for Enhanced Uniformity of Mist-CVD Ga_2O_3 Thin Film," J. Semiconductor & Display Technology, Vol. 21, No. 4., pp. 81-85, 2022.
12. Keswani, M., Raghavan, S., and Deymier, P., "A Novel Way of Detecting Transient Cavitation near a Solid Surface During Megasonic Cleaning using Electrochemical Impedance Spectroscopy," Microelectron. Eng., Vol. 108, pp. 11-15, 2013.
13. Hauptmann, M., Brems, S., Camerotto, E., Zijlstra, A., Doumen, G., Bearda, T., Mertens, P. W., and Lauriks, W., "Influence of Gasification on the Performance of a 1 MHz Nozzle System in Megasonic Cleaning," Microelectron. Eng., Vol. 87, No. 5-8, pp. 1512-1515, 2010.
14. Kim, H., Lee, Y., and Lim, E., "Design and Fabrication of an L-type Waveguide Megasonic System for Cleaning of Nano-scale Patterns," Current Applied Physics, Vol. 9, pp. e189-e192, 2009.
15. Chu, C.-L., Lu, T.-Y., and Fuh, Y.-K., "The Suitability of Ultrasonic and Megasonic Cleaning of Nanoscale Patterns in Ammonia Hydroxide Solutions for Particle Removal and Feature Damage," Semiconductor Science and Technology, Vol. 35, No. 4, p. 045001, 2020.
16. Ochiai, N. and Ishimoto, J., "Numerical Analysis of Single Bubble Behavior in a Megasonic Field by Non-spherical Eulerian Simulation," ECS Journal of Solid State Science and Technology, Vol. 3, No. 1, pp. N3112-N3117, 2014.
17. Han, Z., Keswani, M., Liebscher, E., Beck, M., and Raghavan, S., "Analysis of Sonoluminescence Signal from Megasonic Irradiated Gas-containing Aqueous Solutions using Replaceable Single-band Filters," ECS Journal of Solid State Science and Technology, Vol. 3, No. 1, pp. N3101- N3105, 2014.
18. Li, K., Li, C., Wang, T., Zhao, D., and Lu, X., "Mechanism Analysis of Megasonic and Brush Cleaning Processes for Silicon Substrate after Chemical Mechanical Polishing," ECS Journal of Solid State Science and Technology, Vol. 11, No. 10, p. 104004, 2022.
19. Zhang, L., Lu, X., and Busnaina, A. A., "Non-contact Post-CMP Megasonic Cleaning of Cobalt Wafers Materials," Science in Semiconductor Processing, Vol. 156, No. 15, p. 107278, 2023.

접수일: 2023년 7월 12일, 심사일: 2023년 9월 5일,
게재확정일: 2023년 9월 5일